JOURNAL OF CATALYSIS 86, 147–157 (1984)

Multitechnique Analysis of a Deactivated Resid Demetallation Catalyst

T. H. FLEISCH,* B. L. MEYERS,* J. B. HALL,* AND G. L. OTT†

*Standard Oil Company (Indiana), Amoco Research Center, Box 400, Naperville, Illinois 60566 and †Amoco Oil Company, Amoco Research Center, Box 400, Naperville, Illinois 60566

Received February 18, 1983; revised October 18, 1983

A spent resid demetallation catalyst has been characterized using kinetic analysis, N_2 adsorption, X-ray photoelectron spectroscopy (XPS or ESCA), elemental analysis, X-ray diffraction (XRD), electron microprobe analysis, and CO chemisorption. During the demetallation process Ni, V, Fe, S, and C deposited from the resid feed onto the catalyst surface leading to its deactivation. The catalyst accepted about 100% of the original catalyst weight as metals and coke. Surface areas dropped by 30–65% and pore volumes were reduced by 60–85%. The deposition of metals, sulfur, and coke takes place preferentially at the entrances of pores, causing pore mouth plugging. This effect can be semiquantitatively described by the constraint index which is obtained by division of the N_2 adsorption/desorption hysteresis loop area by pore volume. All elements exhibit preferential deposition on the catalyst extrudate surfaces as evidenced by XPS and by electron microprobe extrudate cross-section analyses. Vanadium and nickel sulfides are formed on the working catalyst surface. The sulfides have been identified as V_3S_4 and Ni_3S_2 or Ni_2S. Upon air exposure these sulfides oxidize slowly on the surface. Nickel and vanadium deposition through the reactor bed parallel each other with a maximum deposition at about 17% of bed depth, whereas the carbon profile is relatively uniform. The top section of the catalyst bed, containing 1.5 times the metals but 0.9 times the carbon compared to the bottom section, was 30–50% more active for both V and Ni removal.

INTRODUCTION

Removal of trace metals from petroleum residue is a major goal of hydrotreating catalysis. These organically bound trace contaminants tend to foul downstream catalytic processes or deposit in industrial boilers when the resid is burned. Recently, a new family of catalysts, tailored specifically for the demetallation reaction has been developed (*1, 2*). Understanding how these catalysts function and deactivate requires careful characterization of the spent material.

The purpose of this paper is to report on the characterization of a spent resid demetallation catalyst using kinetic analysis, N_2 adsorption, CO chemisorption, electron microprobe analysis, X-ray diffraction (XRD), X-ray photoelectron spectroscopy (XPS or ESCA), and elemental analysis. Each technique provides information relevant to the physical and chemical makeup of the working demetallation catalyst.

EXPERIMENTAL

Sample preparation. Fresh resid demetallation catalyst containing 1% MoO_3 on a large pore Al_2O_3 support, prepared according to Ref. *3*, was used to hydroprocess an Ardeshir vacuum resid with properties shown in Table 1. The high pressure fixed bed reactor, containing 2500 cm^3 of catalyst in a 12-ft bed, operated down flow with pure hydrogen and vacuum resid feed entering the top. The reactor operated adiabatically to simulate a commercial fixed bed reactor and therefore had an ascending temperature profile throughout the run. Inlet temperature to the catalyst bed was steadily increased, as the catalyst deactivated, to achieve 50 wt% vanadium removal throughout the run. The run was terminated when increasing temperature no

0021-9517/84 $3.00

TABLE 1

Feedstock Properties—Ardeshir Volume Resid

Gravity, °API	4 0
Sulfur, wt%	5 2
Carbon, wt%	83 74
Hydrogen, wt%	9 90
Nitrogen, wt%	0 484
Oxygen, wt%	0 364
Vanadium, ppm	229
Nickel, ppm	62
Asphaltenes, wt%	14 3
Ramscarbon residue, wt%	26 3

longer improved demetallation performance

At the conclusion of the run, the reactor temperature was lowered before switching from the resid feed to gas oil While on gas oil, the catalyst was cooled to room temperature and then washed in toluene Catalyst was vacuumed from the top of the unit in sections Prior to analysis, each section was chloromethane washed in a Soxhlet extractor for 24 hr and dried overnight in vacuum at 38°C Samples are numbered from the top of the bed, 1 through 14 Catalyst sections from 9% (Section 6) and 73% (Section 13) of the bed length from the top, were designated as "top" and "bottom " They were carefully characterized and used in kinetic studies The kinetic work was conducted in a bench scale isothermal fixed bed unit After loading, the test sample was presoaked in gas oil at 65°C overnight The catalyst then hydroprocessed gas oil feed for 2 days prior to introduction of resid

Sample characterization The specific surface area in square meters per gram and the pore size distribution from 10 to 600 Å radius were calculated from nitrogen adsorption/desorption isotherms obtained at liquid nitrogen temperature on an automated Digisorb 2500 (Micromeritics Instrument Corporation) Approximately 150 mg of sample was pretreated at 250°C and less than 10^{-4} Torr for 6 hr The BET equation was employed to calculate specific areas (*4*) Pore size distributions were calculated using the method of Roberts (*5*) The degree of pore mouth plugging was calculated using adsorption/desorption hysteresis loops and by a novel procedure described more fully elsewhere (*6*) Briefly, the total area subtended by the hysteresis loop is divided by the total pore volume The multiple is called a "constraint index " The greater the index, the greater the departure from uniform cylindrical pores

The XPS measurements were performed with a Hewlett-Packard (HP) 5950B spectrometer using monochromatic Al$K\alpha$ radiation ($h\nu$ = 1486 6 eV) Low energy electrons supplied by an electron flood gun minimized sample charging The recorded photoelectron binding energies were referenced against the C 1s line at 284 6 eV as suggested by Wagner (*7*) The validity of this reference in our catalyst system was established by the achievement of a constant Al 2p photoelectron binding energy of 74 3 ± 0 2 eV on all sample surfaces A value of ~74 2 eV is characteristic for Al in γ-Al_2O_3 (*8–10*)

A JEOL electron microprobe measured the Ni, V, C, Fe, S, and Cr concentration as a function of radial position in individual catalyst extrudates The specimens were prepared by embedding six or seven extrudates of each catalyst in epoxy mounts The embedded extrudates, which were orientated parallel to each other and normal to the base of the embedding mold, were ground and polished to expose smooth cross sections normal to their axial direction Silver paint provided an electrical path from the sample surface to ground

RESULTS AND DISCUSSION

Nickel, Vanadium, and Coke Profiles versus Bed Depth

Figure 1 shows the spent catalyst nickel, vanadium, and carbon concentration as a function of bed depth Nickel and vanadium deposition parallel each other very closely on the macro scale with maximum

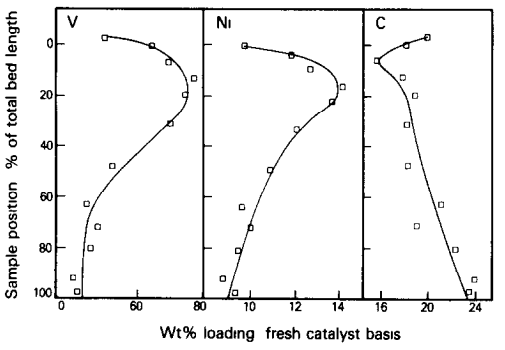

FIG 1 V, Ni, and C concentration profiles in wt% (fresh catalyst baiss) at the end of demonstration run 0 = top of bed, 100 = bottom of bed

deposition occurring at about 17% of bed depth Several phenomena could result in the observed maximum vanadium and nickel concentration A consecutive mechanism of resid demetallation, where metal bearing asphaltenes are first cracked to form resins which subsequently demetallate, is one possible explanation The top 10–20% of the catalyst bed could function primarily as an asphaltene cracking section As new metal bearing resins are generated, the demetallation rate increases until the supply becomes depleted and the exponential decline in deposition occurs Other possible explanations include nonisothermality or unusual deactivation behavior near the top of the bed However, we found that the position of the maximum does not change throughout the run If severe deactivation had occurred as metals accumulated, the maximum would proceed down the bed as a wave

The carbon profile is relatively uniform at start of run, however, end of run analysis shows a steadily increasing carbon level down the catalyst bed as shown in Fig 1 The ascending coke profile is an indirect result of adiabatic operation The catalyst bed operated with a 15 to 20°C temperature rise (with H_2 quench) Near the end of run, the programmed temperature increases at the reactor inlet resulted in bottom of bed temperatures exceeding 435°C Excessive temperatures promoted coking reactions resulting in the observed carbon profile on the spent catalyst

Kinetic Analysis of the Top and Bottom Sections

A detailed elemental analysis of the top and bottom sections is shown in Table 2 The top section contains 1 5 times the metals but 0 9 times the carbon compared to the bottom section Kinetic studies on these two sections were performed to relate the differences in composition to reactivity These were done at two temperatures (404 and 415°C) and at three oil feed rates, space velocities, (1 5, 1 0, 0 5 hr^{-1}) which provided the basis of the relative activity and activation energy calculations The test feed was Ardeshir vacuum resid with properties listed in Table 1

A first-order model was used to calculate the relative activity at reference conditions throughout the run Straightline deactivation was assumed between reference condition periods to calculate the catalyst activity at each set of operating conditions relative to the beginning of the test run and adjust the kinetic plots accordingly Corrections to the 1/LHSV term were never more than ±15%

Figures 2 and 3 illustrate vanadium and nickel removal kinetics for the top and bottom sections Weight fraction of Ni and V

TABLE 2

Elemental Analysis of Top and Bottom Sections

	Top (9% from top)	Bottom (73% from top)
Bulk density g/cm³	1 35	1 08
	wt% (fresh catalyst basis)	
Ni	14 1	10 4
V	77 0	52 3
Fe	3 2	1 0
S	58 5	36 4
H	1 0	1 4
N	5	4
C	17 7	19 9
Ni + V + Fe	94 3	63 7

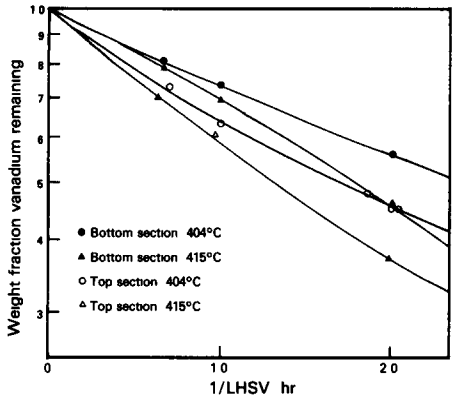

FIG 2 Vanadium removal kinetics LHSV = liquid hourly space velocity

TABLE 3

Demetallation Kinetic Comparison—Top vs Bottom[a]

Conversion	E_a Top	E_a Bottom	A_{Top}/A_{Bottom} 404°C	A_{Top}/A_{Bottom} 415°C
		Vanadium		
0 3	13 3	14 8	1 43	1 34
0 4	17 5	19 7	1 47	1 43
0 5	21 1	26 3	1 52	1 50
		Nickel		
0 2	11 1	13 8	1 47	1 43
0 3	13 1	22 3	1 50	1 34
0 4	19 7			1 26

[a] E_a, activation energy (kcal/gmole), A, activity

remaining is plotted versus reciprocal space velocity Table 3 compares activation energies and activities of the two sections at various levels of conversion The top section of the catalyst bed is 30–50% more active than the bottom section for both vanadium and nickel removal The apparent activation energy for vanadium removal ranges from 13 3 to 26 3 kcal/gmole and increases with severity A similar trend occurs with de-nickelation The shifting apparent activation energy emphasizes the complexity of the reaction kinetics Several processes including catalytic reaction, diffusion, and thermal reaction can contribute to the observed rate

Surface Area and Pore Size Distributions

Table 4 compares the total surface area and pore volume from nine progressively deeper sections of the catalyst bed to the fresh catalyst values Two facts are immediately clear These catalysts, which accepted about 100% of the original catalyst weight as metals and coke, have significantly altered structures Pore volumes have been reduced by 60–85% and surface areas by 30–65% Both values show extensive alteration of the catalyst

Second, the preferential use of the top portions of the bed is obvious as shown by the regular increase in surface area and pore volume with bed depth Relative pore size distribution of fresh and used catalysts are shown by histograms in Fig 4 The se-

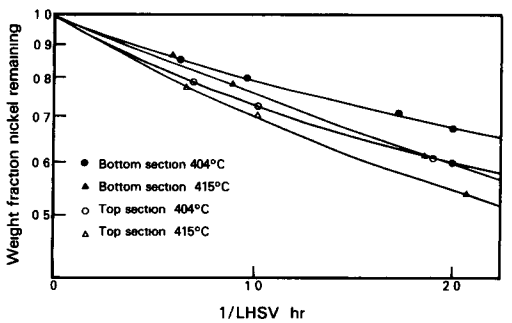

FIG 3 Nickel removal kinetics LHSV = liquid hourly space velocity

TABLE 4

Changes of Surface Area and Pore Volume Through Reactor Bed

Section	Surface areas (m^2/g fresh cat)	Surface areas (% of fresh)	Pore volume (% of fresh)
Fresh	188	100	100
4	64	34 0	17 9
5	70	37 2	23 8
6 ("top")	79	42 0	28 6
9 ("mid")	93	49 5	34 5
10	104	55 3	42 9
11	131	69 7	44 0
13 ("bot")	133	70 7	45 2
14	130	69 1	41 7

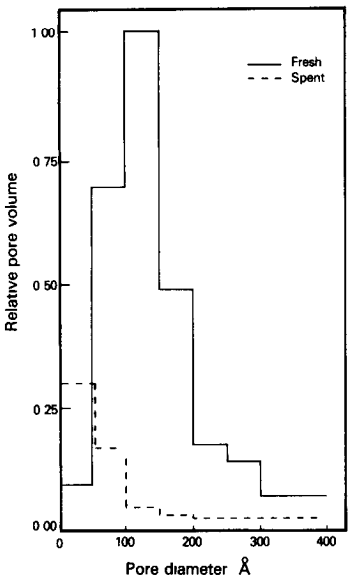

FIG 4 Pore volume distribution of fresh and spent (top) catalyst

vere loss in total pore volume as well as preferential filling of large pores and net increase of pores smaller than 50 Å diameter from larger pores are clearly seen

Pore Mouth Plugging

The nitrogen adsorption/desorption isotherms of fresh and used material (top) are shown in Fig 5 The large increase in the hysteresis loop of the used catalyst relative to its greatly decreased pore volume was considered an indication that deactivation via pore mouth plugging may be operative in these catalysts The rapid deposition of vanadium and nickel sulfides and coke near the catalyst exterior could prevent full utilization of the interior pore volume

In an attempt, to measure, in a semiquantitative manner, the extent of pore mouth plugging, a "constraint index" is calculated as follows The area of the hysteresis loop between N_2 adsorption and desorption isotherms is measured This area is divided by the desorption pore volume

$$\text{"Constraint Index"} = \frac{\text{Hysteresis Loop (Absolute Value)}}{\text{Pore Volume}}$$

Table 5 lists the constraint index of three progressively deeper sections of the catalyst bed in contrast to the fresh catalyst A regular progression is noted showing severe pore mouth plugging at the top of the bed which decreases with bed depth

Table 5 also shows several surface area ratios First of these is the calculated area of pores measured by the desorption process compared to the calculated area of pore measured by the adsorption process If the pores are perfectly uniform cylinders with no pore mouth plugging, we might expect the N_2 desorption/adsorption area ra-

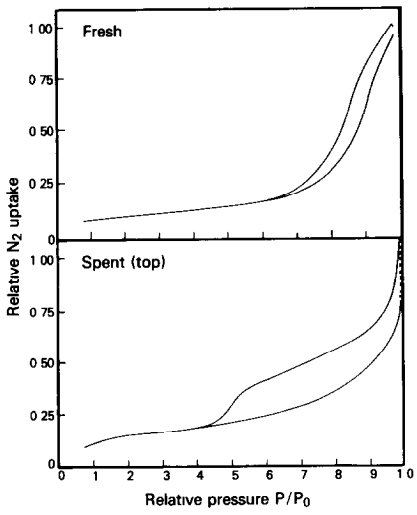

FIG 5 Adsorption–desorption isotherms

TABLE 5

N_2 Adsorption Measurements of Pore Mouth Plugging[a]

Section	Constraint index	D/A	D/BET	A/BET
6	30,200	1 73	1 72	1 00
9	25,600	1 72	1 58	0 92
13	19,500	1 51	1 53	1 02
Fresh	11,450	1 15	1 48	1 28

[a] A = pore area calculated from adsorption data, D = pore area calculated from desorption data, BET = total surface area (experimental)

tio to be close to unity Indeed this is the case for the fresh catalyst where the ratio is 1 15, but the ratio rises to 1 73 at the top of the bed in Section 6 Physisorbed nitrogen in "Inkbottle" pores cannot desorb until the relative pressure is low enough to allow the adsorbed nitrogen in the narrow neck to desorb When this point is reached, the much greater interior volume of the ink bottle is free to desorb and is counted as pores with the diameter of the narrow neck resulting in large desorption/adsorption area ratios The discrepancy between adsorption and desorption surface areas is, therefore, another measure and confirms pore mouth plugging in these upper sections of catalyst bed Still another indication of pore mouth plugging is the ratio of the calculated desorption surface area to the experimentally measured BET surface area This ratio is also seen to be higher in the top portions of the bed

Lastly, in Table 5 there is a column showing the calculated adsorption area ratioed to the experimental determined BET area Here the ratio stays near 1 0 for all used samples because adsorption data measure the "true" composite pore size distribution and are not affected by pore mouth plugging. The nearness to unity and the constancy of this ratio is reassuring that our calculations are correct Note, however, that the fresh sample exhibits a ratio of 1 28 which must result from a pore geometry with only a few simple cylindrical pores The used samples, on the other hand, must have acquired more cylindrical pores as a result of the metal deposition If one wishes to measure "true" pore size distributions in catalysts of this type, we would use adsorption data, but if one wishes to measure "effective" pore size distributions, desorption data are preferred If pore mouth plugging as a deactivation mechanism is to be measured, a hysteresis loop showing both types of data is required and data should be tabulated as in Table 5

Further evidence of pore mouth plugging is the fact that the constraint index decreases from 30,500 to 24,400, when material from Section 6 was investigated after powdering (Table 6) In a similar experiment, a catalyst from Section 9 was tumbled to remove 4% by weight of surface material The residue showed a constraint index of only 22,500 compared to 25,600 from the nonabraded sample as shown in Table 6

TABLE 6

Changes of Constraint Index with Physical Alteration of Sample

Section	Constraint index
6	30,500
6 (powdered)	24,400
9	25,600
9 (4% removed by abrasion)	22,500

Contaminant Metal Surface Area Measurements

Nickel is known to catalyze its own removal as well as the removal of vanadium and sulfur If the rate of nickel and vanadium removal is rapid, pore mouth plugging from deposits near the exterior takes place Therefore, a quantitative measure of active sites for demetallation and desulfurization would be desirable, but is, unfortunately, extremely complex because the "working" demetallization catalyst may exhibit several types of active sites for demetallation associated with Ni, V, Fe, Mo, and the alumina support Some experiments were done employing CO chemisorption to obtain a rough measure of active site density

Catalyst samples were treated in flowing hydrogen at 400°C overnight and swept clean in flowing helium before dosing with CO at room temperature We found that the top section chemisorbs twice as much as the bottom (18 versus 9 μmole CO/g) Undoubtedly, only a portion of all active sites are reduced properly to chemisorb, but the Ni sites are most likely to chemisorb under these conditions Indeed, if one relates CO

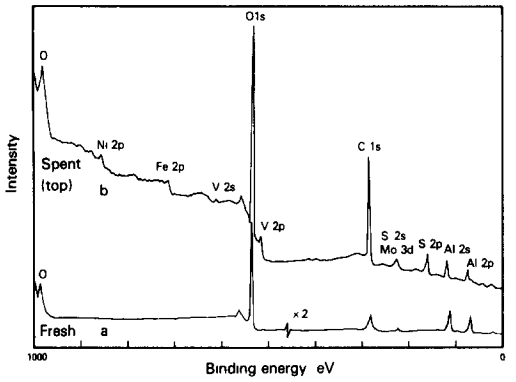

FIG 6 XPS survey spectra of a fresh and spent catalyst

chemisorption to nickel content, the ratio is essentially constant (CO/Ni—0 006) The greater number of active metal sites for demetallation in the top portions of the bed is partially offset by the reduced pore volume and greater pore mouth plugging in these sections These data are consistent with our earlier kinetic finding of a 30–50% higher activity of the top portion of the catalyst

X-Ray Diffraction Studies

Some used catalysts were examined by X-ray diffraction (XRD) A tumbling of the catalyst extrudates to produce a limited amount of abrasion fines from the catalyst exterior showed the vanadium to be present as an unusual V_3S_4 state Nickel sulfides, while likely present in high concentration, were not detected in XRD patterns

Surface Analysis by XPS

The catalyst for resid demetallation has been used in an extruded form The extrudates were less than 1 mm in diameter and approximately 5 mm long They were analyzed by XPS in two different ways First, a few extrudates were mounted parallel on a sample holder to expose the "external" surface to the XPS analysis Second, some extrudates were ground and the resulting powder pressed into a pellet thereby exposing mainly the "interior" surfaces of the extrudates In both cases, no particular precautions were taken to avoid air exposure

Surface Composition

The changes in elemental composition between a fresh and a spent catalyst are illustrated in Fig 6 comparing their XPS survey spectra Keeping in mind the detection limit of ~1 atom% (under the instrumental conditions of a survey scan) and the incapability of hydrogen detection by XPS we find the deposition of vanadium, nickel and iron along with sulfur and carbon on the catalyst Spectrum b in Fig 6 (spent catalyst) was obtained from Section 6 (in pellet form) The relative amounts of the deposited materials vary through the reactor bed as already discussed Significant differences in the survey spectra are also observed between the exterior and interior extrudate surfaces

Table 7 lists "surface compositions" of 3 different catalyst sections each analyzed as the original extrudate and as pellet The analysis was done using the C 1s, O 1s, Al 2p, S 2p, Ni 2p, V 2p, and Mo 3d line A linear background was subtracted from the spectra to attempt to discount the inelastically scattered electrons After a five-point smoothing operation, the spectral areas were obtained by computer integration They were normalized for all instrumental parameters as well as photoionization cross sections, $\sigma(E)$, and for differences in electron mean paths, $\lambda(E)$ We relied on the values for $\sigma(E)$ calculated by Scofield (*11*) The correction for different escape depths was done by assuming that the mean free paths, $\sigma(E)$, vary as the square root of the photoelectron kinetic energy in the region from 200 to 1400 eV (*12*) The peak areas were normalized relative to a kinetic energy of 1000 eV With all these corrections, these numbers represent a "surface composition" averaged over the first few monolayers with exponentially decreasing contribution from the first to deeper lying layers These numbers prove to be useful in comparing relative changes among similar sam-

TABLE 7

Surface Composition of Spent Demetallation Catalysts Expressed in Atomic Ratios Relative to Al and in Relative Weight Percent

	Atomic ratio								Weight percent							
	Al	S	C	O	Ni	V	Fe	Mo	Al	S	C	O	Ni	V	Fe	Mo
#6																
Pellet	1	0 53	3 90	3 20	0 04	0 19	0 04	0 06	16 8	10 6	29 1	31 4	1 3	5 9	1 3	3 7
Extrudate	1	17 90	208 9	61 10	0 90	3 50	1 10	2 10	0 6	12 5	54 7	21 3	1 2	3 9	1 3	4 3
#9																
Pellet	1	0 93	4 40	3 50	0 09	0 39	0 05	0 03	13 8	15 2	26 7	28 7	2 6	10 2	1 5	1 5
Extrudate	1	26 90	193 30	85 0	0 94	2 30	0 50	2 40	0 5	17 2	46 4	27 2	1 1	2 4	0 6	4 6
#13																
Pellet	1	0 54	3 70	3 40	0 06	0 25	0 04	0 04	16 3	10 4	26 7	33 1	2 0	7 7	1 2	2 5
Extrudate	1	10 70	94 40	33 30	0 46	2 10	0 53	0 50	1 2	15 2	50 5	23 7	1 2	4 8	1 3	2 1

ples (*13*) Table 7 shows significant differences in the surface composition of extrudate exterior and interior The most apparent difference is the lack of a strong Al signal from the external surfaces because of a thick carbon/metal sulfide overlayer which attenuates the Al photoelectrons Carbon concentrations between 45 and 55 wt% are found on these samples compared to about 28 wt% on the pelletized samples This observation points to the not unexpected fact that the extrudate surface is more severely coked than its interior, most likely due to diffusional effects, as indicated by the pore size data

Very interesting are the Mo/Al atomic ratios shown in Table 7 When contaminant metals, sulfur and coke are deposited on the catalyst surface during time on-stream one would expect that the Mo and Al are buried simultaneously However, as shown in Table 7, overlayer deposition strongly decreases the Al signal on the extrudate surfaces whereas the Mo signal is more or less unaffected by this deposition We, therefore, observe much higher Mo/Al surface atomic ratios on the extrudate than on the pellet surfaces Apparently, the Mo sites either remain uncovered or migrate to the top of the deposited layer

Surface Chemistry

High resolution XPS spectra yield more information on the chemistry of the deposited materials Figure 7 shows V $2p_{3/2}$ spectra of the deactivated catalyst from the top of the reactor A doublet indicates the presence of two chemically different V species The two peak maxima are located at 513 4 ± 0 3 and 516 9 ± 0 2 eV on the binding energy scale indicative of the presence of a V^{2+} or V^{3+} and V^{4+} or V^{5+}, respectively (*7*) The former one may be correlated with a V_3S_4 that has been identified by X-ray diffraction The formal oxidation state of V in this compound is 2 67 (mixed sulfide) This might explain the binding energy of 513 4 eV which is significantly higher than the

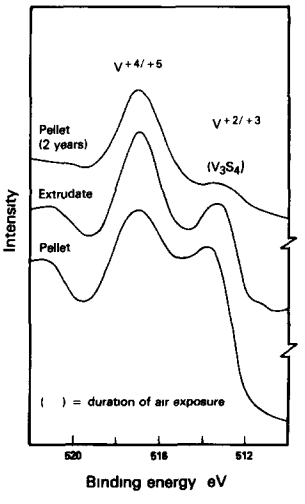

FIG 7 V $2p_{3/2}$ photoelectron lines of section 6 (top)

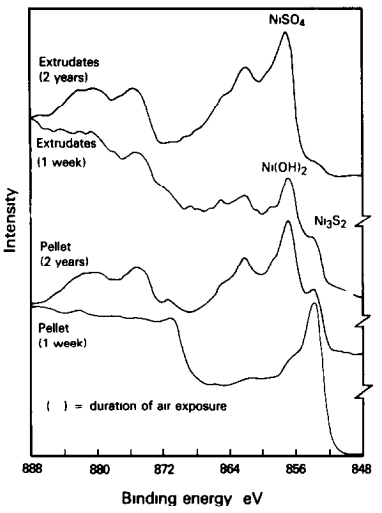

FIG 8 Ni 2p photoelectron lines of section 6 (top)

values reported for V^{2+} compounds However, it is well known that there is a wide spread in binding energies for each particular oxidation state and, therefore, often an overlap between adjacent oxidation states

Supporting the presence of a vanadium sulfide is the S 2p photoelectron binding energy of ±161 7 eV which undoubtedly indicates a sulfide anion (*7*) The presence of a V^{4+} species is surprising considering the strongly reducing environment of the resid demetallation reactor and suggests an air exposure induced artifact Months of room temperature air exposure caused oxidation of V^{2+} to V^{4+} that was complete after 2 years (Fig 7) The presence of any vanadium oxide can be excluded since we do not find the characteristic oxide peak at ~530 0 eV (*14*) The only detectable O 1s species appears at 531 8 eV which is, among others, typical for hydroxides (*15*) We, therefore, believe that the high oxidation state vanadium compound with a $2p_{3/2}$ binding energy of 516 9 eV could be a $V^{4+/5+}$ hydroxide and/or sulfate (we observed the oxidation of S^{2-} into SO_4^{2-} as discussed later) or a more complex, mixed compound as, for instance, a $VOSO_4$ Its V $2p_{3/2}$ binding energy has been reported at 516 0 eV (*16*) which is slightly lower than our value

This demonstration of a sample handling induced artifact underlines the necessity for extreme care in discussing surface chemistry from XPS data of air exposed sample surfaces Because the air oxidation is slow, XPS can identify V_3S_4 as the most likely form of the vanadium deposit on the working catalyst

Nickel is the other major metal removed from resid The Ni level on spent catalyst is 25% of vanadium as shown by elemental analysis (Table 2) and XPS analysis (Table 7) This lower Ni concentration relative to vanadium is the result of a threefold lower Ni content in the feed and an intrinsically slower de-nickelation kinetics The Ni chemistry parallels that discussed for V Nickel deposits on the catalyst surface as a sulfide with a Ni $2p_{3/2}$ binding energy of 853 7 eV (Fig 8) The sulfide form is either Ni_3S_2 (853 7 eV) (*8*) or Ni_2S (854 0 eV) (*8*) The Ni species is clearly not NiS (854 9 eV) (*8*) and not metallic Ni (852 8 eV) (*14*)

Upon air exposure a new Ni species tentatively assigned to $Ni(OH)_2$ slowly forms ($2p_{3/2}$ binding energy of 856 4 eV) as shown in Fig 8 (*15, 17*) After 1 week of air exposure, oxidation has progressed extensively on the extrudate surfaces but has not yet penetrated the extrudate interiors (compare spectra of extrudate and pellet surface) Another chemically feasible compound,

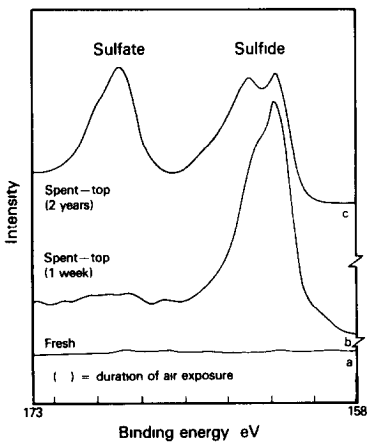

FIG 9 S 2p photoelectron lines of section 6 (top) and of fresh catalyst

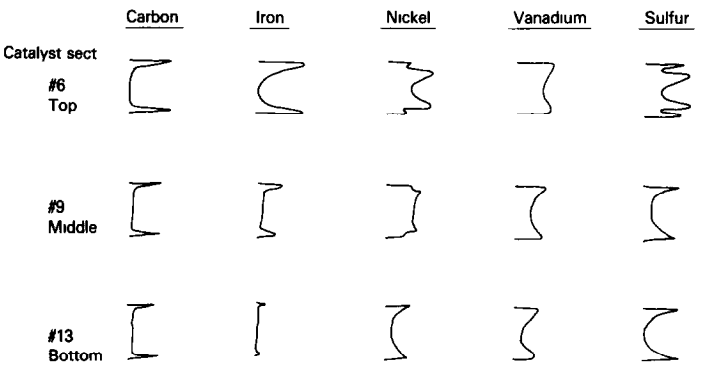

FIG 10 Elemental composition profiles across catalyst extrudates (extrudate diameter is 0 79 mm)

$NiSO_4$, is most likely not present since its Ni $2p_{3/2}$ binding energy is at a significantly higher value of 857 1 eV (*18*) More importantly, the high oxidation state Ni is already observed at a time when all the sulfur is still present as sulfide However, after very long air exposures with significant sulfate quantities present we locate Ni $2p_{3/2}$ at ~857 2 eV indicating the presence of $NiSO_4$

Demetallation of the feed is accompanied by desulfurization Up to 17 wt% sulfur was detected on the catalyst surface (Table 7) As already mentioned, all the sulfur is found with a very low 2p binding energy of 161 7 indicative of metal sulfides Despite air exposure for one week, minimal sulfur oxidation is observed (Fig 9) After 2 years of air exposure, varying amounts of sulfate (30 to 80% of the total sulfur) have formed Figure 9c shows the presence of a sulfate species with a 2p binding energy of ~169 0 eV along with the original sulfide Note the change in the sulfide peak structure, indicative of the additional formation of a different sulfide species with slightly higher binding energy It is the discrepancy in the oxidation rate of metals versus sulfur that indicates a transformation of the deposited metal sulfides into metal oxides/hydroxides rather than into sulfates

Elemental Distribution Profiles by Electron Microprobe Analysis

Figure 10 shows qualitative radial distributions of carbon, iron, nickel, vanadium, and sulfur from three levels of the catalyst bed Carbon and iron are highly concentrated on the extrudate surface, at all levels, indicating poor diffusion through the catalyst Vanadium is slightly concentrated at the extrudate surface, but it is found throughout For the top section (#6), the nickel and sulfur profiles are more complex They show maximum concentrations both at the extrudate surface and about halfway to the center of the extrudate Towards the bottom sections all elements have similar profiles, showing higher concentrations at the extrudate surface The shape of the V, Ni, and S profiles for the top section is consistent with vanadium and nickel being present as sulfides The sulfur profile appears to be a composite of the nickel and vanadium profiles

CONCLUSIONS

Nickel and vanadium deposition through the reactor bed parallel each other closely with a maximum deposition at about 17% of bed depth This points to a consecutive demetallation mechanism where the metal containing hydrocarbons are first catalytically converted into other compounds which then easily demetallate

The coke profile through the reactor bed is relatively uniform Higher temperatures at the bottom of the bed led to increased coke levels

Interesting deposition profiles across the extrudates have been observed for C, Fe,

Ni, V, and S All elements exhibit preferential deposition on the extrudate surface The V, Ni, and S profiles are consistent with the presence of vanadium and nickel sulfide which have been identified as V_3S_4 by XRD and XPS and as Ni_3S_2 or Ni_2S by XPS

Upon air exposure these sulfides slowly oxidize on the surface and form mixed oxides/hydroxides Sulfur originally present as sulfide also oxidizes upon air exposure but more slowly to sulfate

Total surface areas are reduced by 30–65% and pore volumes by 60–85%

The combined deposition of metals, sulfur, and coke takes place preferentially at the entrances of pores leading to pore mouth plugging which can be semiquantitatively described by the "constraint index" obtained by division of hysteresis loop area by pore volume

The top section of the catalyst bed contained 1 5 times the metals but 0 9 times the carbon compared to the bottom section Kinetic analysis showed the former one to be 30–50% more active for both V and Ni removal

REFERENCES

1 Hensley, A L , "Effect of Pore Structure on the Performance of Life and Resid Demetallation Catalysts," Advances in Catalytic Chemistry, Symposium, Salt Lake City, Utah, May 1982

2 Green, D C , and Broderick, D H , "Residium Hydroprocessing in the 80's," Chemical Engineering Progress, December 1981, pp 33–39

3 U S Patent No 4119531

4 Brunauer, S , Emmett, P H , and Teller, E , *J Amer Chem Soc* **60,** 309 (1938)

5 Roberts, B F *J Colloid Interface Sci* **23,** 266 (1967)

6 Meyers, B L , *J Catal* , submitted

7 Wagner, C D , Riggs W M , Davis, L E , Moulder, J F , and Muilenberg, G E , "Handbook for X-Ray Photoelectron Spectroscopy " Perkin-Elmer, 1979

8 Ng, K T , and Hercules, D M , *J Phys Chem* **80,** 2095 (1976)

9 Ogilvie, J L , and Wolberg, A , *Appl Spec* **26,** 402 (1972)

10 Madey, T E , Wagner, C D , and Joshi, A , *J Elect Spectrosc Related Phenomena* **10,** 359 (1977)

11 Scofield, J H , *J Electr Spectrosc Related Phenomena* **8,** 129 (1976)

12 Carlson, T A , "Photoelectron and Auger Spectroscopy " p 262, Plenum, New York, 1975

13 Ott, G L , Fleisch, T , and Delgass, W N , *J Catal* **60,** 394 (1979)

14 Fleisch, T , Winograd, N , and Delgass, W N , *Surf Sci* **78,** 141 (1978)

15 Kim, K S , Baitinger, W E , Amy, J W , and Winograd, N , *Elect Spectrosc* **5,** 351 (1979)

16 Larsson, R , Folkesson, B , and Schoen, G , *Chem Scr* **3,** 88 (1973)

17 McIntyre, N S , Rummery, T E , Cook, M G , and Owen, D , *J Electrochem Soc* **123,** 1165 (1976)

18 Matienzo, L J , Yin, L O , Grim, S O , and Swartz, W E , *Inorg Chem* **12,** 2764 (1973)